Investigations of $Sr_3Fe_{2-x}Mn_xO_{7-\delta}$ the $n=2$ Ruddlesden–Popper phases with d^3/d^4 interactions

Gabriel M. Veith[a], Ian D. Fawcett[a], Martha Greenblatt[a,*], Mark Croft[b], Israel Nowik[c]

[a]*Department of Chemistry Rutgers, The State University of New Jersey, Piscataway, NJ 08854-8087, USA*
[b]*Department of Physics, The State University of New Jersey, Piscataway, NJ 08854-8019, USA*
[c]*Racah Institute of Physics, The Hebrew University, Jerusalem, 91904 Israel*

Dedicated to Professor Bernard Raveau on the occasion of his 60th Birthday

Abstract

We have prepared a series of Mn substituted strontium ferrates, $Sr_3Fe_{2-x}Mn_xO_{7-\delta}$ where $x=2/3$, 1 and 4/3, and investigated their properties with X-ray diffraction, X-ray absorption near edge spectroscopy (XANES), Mössbauer spectroscopy, variable-temperature resistivity and magnetic susceptibility. These compounds are metastable and have to be prepared at high temperatures, >1250°C, with solid state techniques followed by quenching in air to room temperature. As a consequence the compounds are oxygen deficient and contain some Fe^{3+}. They are insulators and exhibit spin-glass like behavior at low temperatures due to frustrated magnetic interactions between the disordered array of transition metal ions on the B site. Mössbauer and XANES spectra show that the B cations are not fully oxidized and that the Fe^{4+} in these compounds are charge-disproportionated into Fe^{3+} and Fe^{5+} at low temperature. © 2000 Elsevier Science Ltd. All rights reserved.

1. Introduction

With the discovery of colossal magnetoresistance (CMR) in manganates [1], such as: $Ln_{1-x}A_xMnO_3$ [2] (Ln=rare earth, A is a divalent cation), and Ruddlesden–Popper (RP) manganates [3], $AO(AMnO_3)_n$, considerable energy has been invested in studying and understanding the CMR phenomenon. These manganates undergo a transition from an insulating, paramagnetic state at high temperatures to a metallic, ferromagnetic (FM) state at low temperature. The application of a magnetic field near the transition temperature T_c induces a large decrease in the resistance in these materials. The CMR, defined as $(\rho_H - \rho_0)/\rho_H$ where ρ_H is the resistance of a compound in a magnetic field and ρ_0 is the resistance without a magnetic field, in the manganates is negative. The magnetic and electronic properties have been explained by the double-exchange (DE) theory, proposed by Zener in 1951 [4]. According to this mechanism, motion of electrons between neighboring Mn^{3+} (d^4) and Mn^{4+} (d^3) occurs via the overlap of Mn-3d-e_g and O-2p orbitals in the Mn^{3+}–O–

Mn^{4+} sub-lattice. The electron transport and the ferromagnetic alignment of the electrons in the underlying Mn-3d-t_{2g} orbitals is mutually enhanced leading to the observed transition to a metallic and ferromagnetic state.

$AO(ABO_3)_n$, RP phases with $n=1$, 2 and 3 are two dimensional layered compounds with a rock salt layer (AO) separating n number of (ABO_3) perovskite layers (Fig. 1) [5]. The perovskite structure is the $n=\infty$ end member of the RP series. Recently, some RP manganates such as $Sr_{1.8}La_{1.2}Mn_2O_7$ were reported to exhibit CMR effects in excess of 200%, at low magnetic fields of $0.3T^3$ [3]. These CMR values are considerably higher than those observed for most perovskite ($n=\infty$) manganates at such low fields [3].

One of the most recent attempts to understand and improve the CMR properties of these manganates was the investigation of oxides containing other d^3/d^4 cations similar to those in manganates, for example substitution of isoelectronic ions, such as Cr^{3+} (d^3) and Fe^{4+} (d^4), for $Mn^{3+/4+}$. In principle, this would replicate d^3/d^4 interactions similar to those seen in perovskite manganates. Gundakaram et al. [6] doped Cr^{3+} (effective ionic radius of Cr^{3+} ($r_{Cr^{3+}}=0.76$ Å) [7]), which is isoelectric with
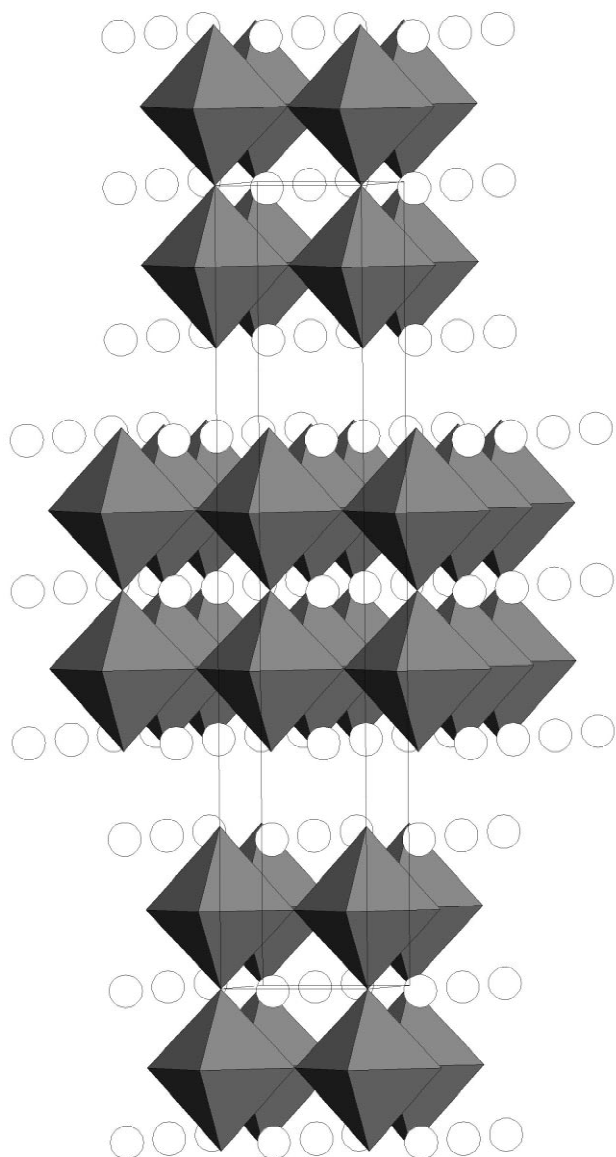
Fig. 1. The $n=2$ Ruddlesden–Popper Structure. The shaded octahedra are Fe/Mn–O_6 and the circles are Sr atoms.

Mn^{4+} into $LnMn^{3+}O_3$; although they found FM superexchange interactions in $LnMn_{1-x}Cr_xO_3$, the compounds were insulating at room temperature and did not exhibit metallic behavior at low temperatures. Battle et al. [8] studied substituted Fe^{4+} phases in the $n=3$ RP member $Sr_4MnFe_2O_{10}$, since Fe^{4+} is isolectronic with Mn^{3+}. However, these compounds did not show a transition to a

metallic state and were oxygen deficient, with both Fe^{3+} and Fe^{4+} in the B-sites, and exhibited complex magnetic interactions such as antiferromagnetic (AF) order and spin-glass like transitions.

The end members of the $n=2$ $Sr_3Fe_{2-x}Mn_xO_7$ family, $Sr_3Fe_2O_7$ and $Sr_3Mn_2O_7$ have been previously synthesized. $Sr_3Fe_2O_7$ was prepared at high pressures, 500 atm O_2 at 500°C, and characterized by several groups [9–12]. The synthesis of pure $Sr_3Fe_2O_7$ requires high oxygen pressure; otherwise it is oxygen deficient. $Sr_3Fe_2O_7$ is semiconducting and orders AF at 100 K. $Sr_3Fe_2O_7$ also undergoes a charge disproportionation according to: $2Fe^{4+} \rightarrow Fe^{3+}$ and Fe^{5+} below 100 K [11]. The $n=2$ manganate compound is more difficult to prepare [13]. $Sr_3Mn_2O_7$ is metastable and decomposes between 1000 and 1600°C into α-Sr_2MnO_4 and $Sr_4Mn_3O_{10}$ [13]. The reactants must be sintered at 1650°C and quenched in dry ice in order to obtain a pure phase. $Sr_3Mn_2O_7$ orders antiferromagnetically at 160 K and is an insulator.

In this paper, we present the results of the synthesis of manganese substituted $n=2$ RP phases of $Sr_3Fe_{2-x}Mn_xO_{7-\delta}$ as well as their electronic and magnetic properties, which were investigated with temperature dependent resistivity and magnetic susceptibility measurements, X-ray absorption near-edge spectroscopy (XANES) and Mössbauer spectroscopy.

2. Experimental

2.1. Synthesis

Stoichiometric amounts of Fe_2O_3 (Fisher Certified, 99+%), MnO_2 (Fisher Certified, 99+%) and $SrCO_3$ (Cerrac 99.5%) were well ground in an agate mortar and pressed into pellets. Details of the synthetic procedures are presented in Table 1. All samples were quenched in air directly from the furnace. The products were gray and are sensitive to moisture. Samples were stored in a dry box or sealed in Pyrex tubes under vacuum.

2.2. Structure

Powder X-ray diffraction data was collected with a Scintag PAD V diffractometer using CuKα radiation, and a Li-drifted germanium detector. Data was collected over a range of $2° \leq 2\theta \leq 120°$, with a step size of 0.02°. Samples

Table 1
Synthetic procedures used for $Sr_3Fe_{2-x}Mn_xO_{7-\delta}$

x	Synthetic conditions	Number of intermittent grindings
2/3	1000°C, 24 h, 1250°C, 96 h; 1300°C, 72 h; quench in air	5
1	1000°C, 24 h; 1250°C, 96 h; 1300°C, 7 d; 1350°C, 24 h; quench in air	8
4/3	1000°C, 24 h; 1300°C, 72 h; 1400°C, 48 h; quench in air	5

were intimately mixed, ground with silicon as an internal standard, and were placed on a glass slide with petroleum jelly. Lattice parameters were calculated by Rietveld refinement with the program GSAS [14].

2.3. Magnetic properties

Temperature-dependent magnetic susceptibility, χ, measurements were made with a Quantum Design SQUID magnetometer (MPMS). The susceptibility data were collected after cooling the sample from 5 to 300 K in the absence (ZFC) and with an applied magnetic field (FC) of 100 gauss, respectively.

2.4. Electrical properties

Temperature-dependent electrical resistivity, ρ, measurements were carried out using a standard 4-point probe technique in a closed-cycle helium refrigerator (ADP Cryogenics). Gold wires were attached to the polycrystalline samples using conducting silver paint from GC electronics.

2.5. Oxygen content

The oxygen content was determined with the iodometric method, described by Licci et al. [15]. Approximately 0.02 g of compound was dissolved in 1.0 M KI and 2.0 M HCl under a nitrogen blanket and titrated against a standardized solution of thiosulfate.

2.6. Electron dispersive X-ray analysis (EDAX)

EDAX was preformed on randomly selected crystallites to verify homogeneity of the samples using an Amray 1400 SEM run at 20 KeV with a magnification of $100\times$.

2.7. Thermogravimetric analysis (TGA)

TGA was performed with a TA Instrument 2050 thermal analyzer.

2.8. X-ray absorption spectroscopy

The Mn and Fe K-edge XANES measurements were performed on beam lines X-19A and X-18B at the Brookhaven national synchrotron light source using a crystal and channel cut Si (*111*) monochromators respectively. Fluorescence and transmission mode measurements were made and checked for consistency. The relative energies between various spectra were established by careful comparison of the simultaneously collected standard spectra. Particular care was taken to use an identical standard sample, which was maintained in a constant position to accurately calibrate the chemical shift results. In general, the relative accuracy of the energy is about

± 0.05 eV. All spectra were normalized to unity step in the absorption coefficient from well below to well above the edge.

2.9. Mössbauer

The Mössbauer studies were performed with a ^{57}Co:Rh source (50 mCi) and a conventional constant acceleration Mössbauer drive. Spectra of four samples (the fourth is an oxygen poor sample, $x = 4/3$, $\delta = 0.34$) were collected at 4.2 and 200 K. The spectra were analyzed and least square fitted by a computer program which allowed a Gaussian distribution of magnetic hyperfine fields in the 4.2 K spectra, and a quadrupole interaction distribution in the 200 K spectra.

3. Results

Reitveld refinements of the lattice parameters were carried out in the space group *I4/mmm* with atomic positions taken from Dann et al. [10] The X-ray diffraction pattern of $Sr_3Fe_{4/3}Mn_{2/3}O_{6.80}$ including the raw data, the fitted profile and the difference plot is given in Fig. 2. Each sample contains small amounts of impurities, which were determined to be α-Sr_2MnO_4 and $Sr_4Mn_3O_{10}$. Impurity peaks were less than 5% of the maximum peak. A progressive decrease of the unit cell dimensions with increasing x is observed. The unit cell parameters of the samples compare well with the previous work on the $n = 2$ end members $Sr_3Fe_2O_{6.56}$ and $Sr_3Mn_2O_7$ (Table 2) [10,13]. The decrease in the unit cell volume with increasing x is consistent with the substitution of the larger Fe^{3+}/Fe^{4+} ($r_{Fe^{3+}/Fe^{4+}} = 0.785/0.72$ Å) [7] for the smaller Mn^{4+}, ($r_{Mn^{4+}} = 0.67$ Å) [7] at the B site. Due to the
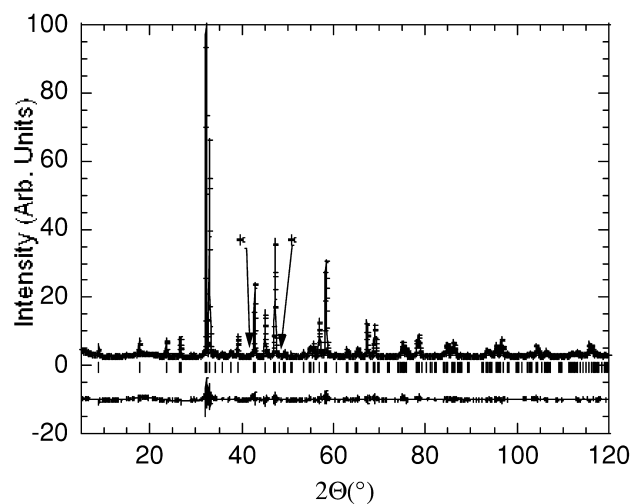
* = Impurities

Fig. 2. Observed (+), calculated (solid line) and allowed reflections (tic) X-Ray diffraction data for $Sr_3Fe_{4/3}Mn_{2/3}O_{6.81}$. Difference plot is at the bottom.

Table 2
Unit cell parameters for $Sr_3Fe_{2-x}Mn_xO_{7-\delta}$

	$x=0$[a]	$x=2/3$	$x=1$	$x=4/3$	$x=2$[b]
δ	0.42	0.20	0.29	0.16	0.00
$a(\text{Å})$	3.8704	3.8512(6)	3.8442(8)	3.8322(1)	3.7997
$c(\text{Å})$	20.1763	20.1503(9)	20.1306(10)	20.1212(9)	20.0959
Volume (Å^3)	302.241	299.023(15)	297.501(17)	295.495(10)	290.139

[a] Data from Ref. [10].

[b] Data from Ref. [13].

uncertainty in estimating the positional parameters of O atoms with X-rays, meaningful metal to oxygen distances could not be established.

The levels of oxygen nonstoichiometry in the samples (determined with iodometric titrations [15]) are listed in Table 2. To determine the oxygen content we assumed that all the Mn was in the $4+$, and Fe was in a mixture of $3+$ and $4+$ formal oxidation states as done by Battle et al. [8].

To determine if there was a homogeneous distribution of Mn and Fe in the compound EDAX was preformed on a portion of randomly selected crystallites. The area under the EDAX peaks for Fe/Mn, for several grains of the same composition, indicated that the crystals analyzed contained nearly identical amounts of each metal in each crystal, within experimental error ($\pm 1\%$). A plot of EDAX data (i.e., Fe/Mn intensities) for the three different compositions indicated a linear relationship of the intensities of the Fe/Mn peaks consistent with composition.

The temperature dependent molar susceptibilities for all the samples studied are shown in Fig. 3. The high temperature susceptibility (150–300 K) data was fitted to the Curie–Weiss law ($\chi = C/(T - \theta)$), with constants given in Table 3. The experimental Curie constants (C) were compared to theoretical Curie constants, determined with the spin-only formula [moles Mn (Mn^{4+}) + moles Fe (($1 - x(Fe^{3+}) + x(Fe^{4+})$))]. The experimentally determined Curie constants were considerably larger than the theoretically calculated ones. We assumed that all the Fe^{4+} had charge disproportionated into Fe^{3+} and Fe^{5+}. Using a modified spin-only formula, considering only Fe^{3+} and Fe^{5+} to be present, the calculated C's were marginally closer to the experimentally determined C's (Table 3). Similar results were reported by Battle et al. [8] and Adler [11] where the calculated C's were also larger than expected. When $x=4/3$, we observe a broad maximum at 50 K, from a derivative of $1/\chi$ versus T plot (Fig. 3), which indicates a two-dimensional AF correlations. The Weiss constant, θ for $x=2/3$ and 1 are both positive (FM-like), while for $x=4/3$ it is negative (AF-like; Table 3). At low temperatures, there is divergence in the FC and ZFC susceptibilities, typical of spin-glass type behavior seen in other RP phases [8,11].

The temperature dependent resistivity plots (Fig. 4) show that the compounds are insulating at room temperature. The thermal activation energy for conduction (E_a) (Table 3) was determined by plotting the ln (ρ) versus

$1000/T$ and taking the slope of the linear high temperature region between 150 and 300 K (Fig. 4).

The Mössbauer spectra are shown in Fig. 5 (4.2 K) and 6 (200 K). The analysis of the spectra yields two inequivalent iron species corresponding to two different iron valence states, in terms of their isomer shift (IS), quad-
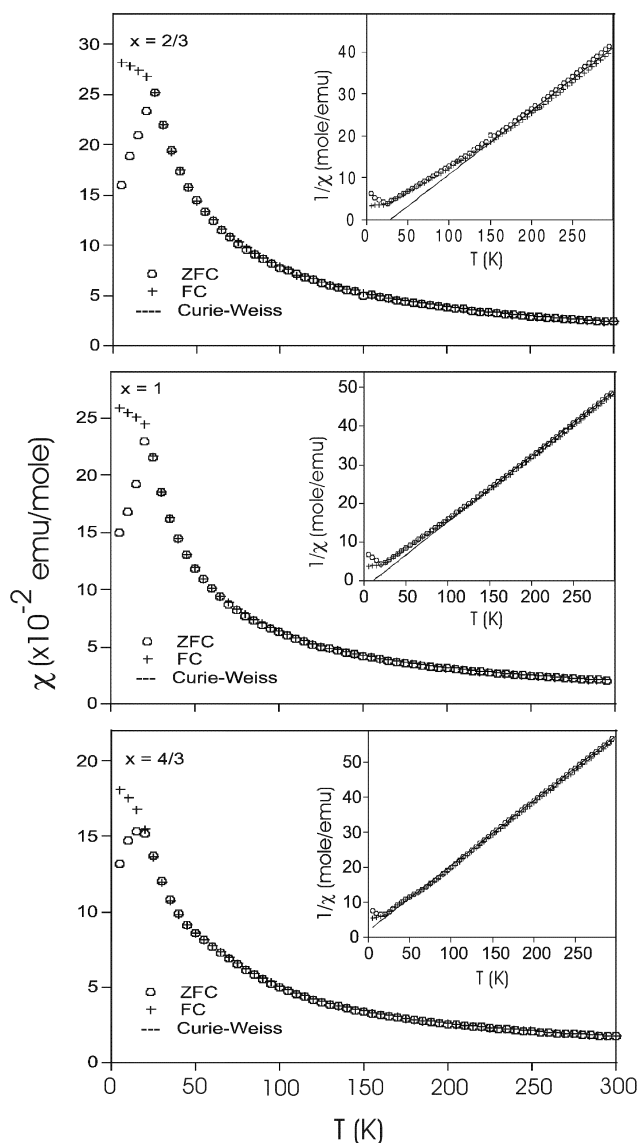
Fig. 3. Temperature-dependent magnetic susceptibility data for $Sr_3Fe_{2-x}Mn_xO_{7-\delta}$. (Inset inverse susceptibility versus temperature).

Table 3
Magnetic and electrical properties of $Sr_3Fe_{2-x}Mn_xO_{7-\delta}$

x	0^a	2/3	1	4/3	2^b
T_g^c(K)	–	25	22	21	–
T_N(K)	100	–	–	50	160
θ(K)	–	28	11	−10	–
$C_{(150–300 K)}^d$ (emu K/mole) (μ_{eff})	–	6.48(7.20)	5.85(6.84)	5.37(6.80)	–
C^e (μ_{eff})	–	5.78(6.80)	5.55(6.66)	4.94(6.29)	–
C^f (μ_{eff})	–	5.89(6.86)	5.61(6.70)	4.98(6.31)	–
$E_{a(150–300 K)}$(eV)	–	0.13	0.14	0.16	–

 a Data from Ref. [10].

b Data from Ref. [13].

c T_g is the spin-glass transition temperature.

d Experimentally determined C and μ_{eff} in brackets; $\mu_{eff} = (8C)^{1/2}$.

e Theoretical C and μ_{eff} assuming the presence of Fe^{4+}.

f Theoretical C and μ_{eff} assuming disproportionation of Fe^{4+} to Fe^{3+} and Fe^{5+}.

rupole splitting (E_Q), and magnetic hyperfine field (B_{hf}); all are given in Table 4. In the 4.2 K spectra the first site, (I), is almost certainly Fe^{3+}, all parameters are identical to those measured for dilute iron in $EuMnO_3$, and the second site, (II), corresponds probably to Fe^{5+}, since the spectra look extremely similar to those observed in $Sr_3Fe_2O_7$ [12], in $CaFeO_3$ [16] and in $LaSr_2Fe_3O_9$ [17] at low temperatures, where the spectra were analyzed as corresponding to Fe^{3+} and Fe^{5+}. The 4.2 K Mössbauer spectra exhibit magnetic hyperfine field distributions and zero quadrupole interactions, while the 200 K (well above the magnetic ordering temperature) data show only large quadrupole interactions (Figs. 5 and 6). This indicates that the samples are in a spin-glass-ordered state at the low temperatures consistent with the magnetic results. The oxygen poor sample $x = 4/3$, $\delta = 0.34$, exhibits a single site (I) both at 4.2 and 200 K. The assignment of Fe^{3+} to this spectrum is fully consistent with the amount of oxygen in this sample (assuming Mn^{4+}). For the other spectra, the amount of

oxygen is not consistent with the Mössbauer sub-spectra relative intensities, neither if $3+$ and $5+$ valences are assigned to the iron, nor for $3+$ and $4+$ valences. Good agreement is obtained only if it is assumed that the second iron site corresponds to an intermediate valence of about $4.5+$ and somewhat temperature dependent. Another
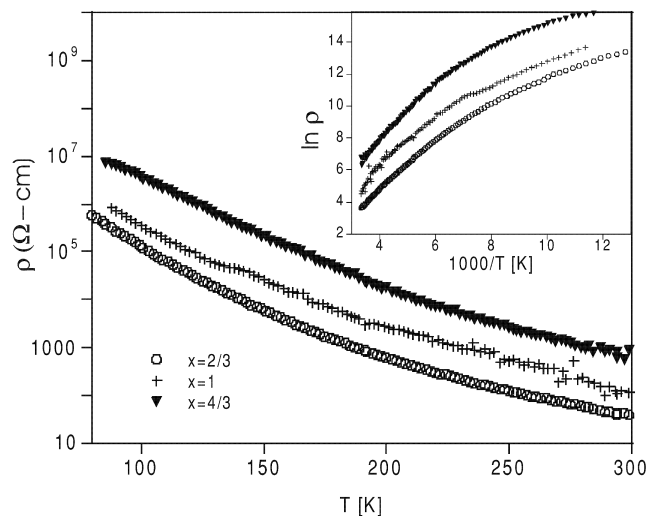
Fig. 4. Temperature-dependent resistivity data for $Sr_3Fe_{2-x}Mn_xO_{7-\delta}$. (Inset ln ρ versus $1000/T$).
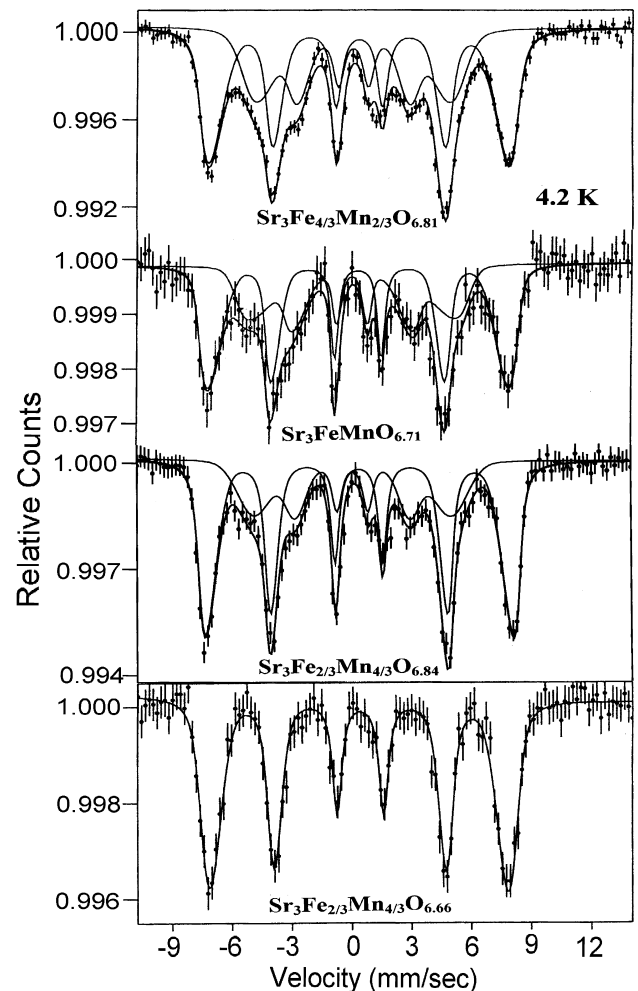
Fig. 5. Mössbauer spectra of ^{57}Fe in $Sr_3Fe_{2-x}Mn_xO_{7-\delta}$ at 4.2 K.

Table 4
Mössbauer parameters for $Sr_3Fe_{2-x}Mn_xO_{7-\delta}$ [a]

		x=2/3		x=1		x=4/3			
	δ	0.19		0.29		0.16	0.34	0.16	0.34
	Temp (K)	4.2	200	4.2	200	4.2		200	
Site 1	IS	0.38	0.30	0.37	0.34	0.39	0.39	0.34	0.35
	ΔE_Q	0.0	0.67	0.0	0.68	0.0	0.0	0.63	0.63
	B_{hf}	486	0.0	480	0.0	490	470	0.0	0.0
	Area (%)	58	68	58	66	65	100	69	100
Site 2	IS	0.09	0.03	0.08	0.05	0.09	–	0.01	–
	ΔE_Q	0.0	0.27	0.0	0.37	0.26	–	0.0	–
	B_{hf}	309	0.0	331	0.0	308	–	0.0	–
	Area (%)	42	32	42	34	35	5	31	10
	ΔIS	0.29	0.27	0.29	0.29	0.31	–	0.32	–
	ΔB	177	–	149	–	182	–	–	–

[a] The IS (± 0.02, relative to iron metal) and ΔE_Q (± 0.02) have units of mm s^{-1}; B_{hf} (± 10) has units of kOe.

possible resolution of this inconsistency is that the iron is indeed 3+ and 5+ but some of the Mn 4+ ions convert to 3+, as some of the XANES spectra tend to indicate. A more plausible possibility, which assumes that the iron

Fig. 6. Mössbauer spectra of ^{57}Fe in $Sr_3Fe_{2-x}Mn_xO_{7-\delta}$ at 200 K.

valences are of intermediate character, is given in the latter discussion.

Fig. 7a and b compare the Fe–K main-edge spectra for α-Fe, Fe^{2+}–FeO, Fe^{3+}–Fe_2O_3, Fe^{4+}–SrFeO$_{3-\delta}$, and $Sr_3Fe_2O_{7-\delta}$. The chemical shift of the steeply rising portion of the main edge between the Fe, Fe^{2+}, Fe^{3+}, and Fe^{4+} standards (Fig. 7a) is apparent. By comparison the $Sr_3Fe_2O_{7-\delta}$ and SrFeO$_{3-\delta}$ spectra fall close to one another and are clearly shifted up in energy relative to the Fe^{3+}–Fe_2O_3 standard spectrum. The Fe–K pre-edge spectra $Sr_3Fe_2O_{7-\delta}$ differs more strongly (than the main edge) from that of SrFeO$_{3-\delta}$ (see Fig. 7b). Although both of these pre-edges manifest a strong single peak, the peak of the $Sr_3Fe_2O_{7-\delta}$ is strongly shifted down in energy and is labeled L1, for clarity, in Fig. 7b.

The Fe composition (x) dependence of the Fe–K main-edge in the $Sr_3Fe_{2-x}Mn_xO_{7-\delta}$ compounds can be seen to be small in Fig. 8a. Two points should be noted regarding the energy of the Mn–K main edge peak for the $Sr_3Fe_{2-x}Mn_xO_{7-\delta}$ ($x=1/3$, 1/ and 4/3) in Fig. 9a: The peaks for these compounds fall between those of the Mn^{3+}–LaMnO$_3$ and the Mn^{4+}–CaMnO$_3$ standards but somewhat closer to the latter standard; and there appears to be little shift of these peaks with varying Fe content x. The Mn–K pre-edge features, related to transitions into final d-states, for these compounds are shown in Fig. 9b.

4. Discussion

Several oxygen deficient $n=2$ RP phases, with the stoichiometry $Sr_3Fe_{2-x}Mn_xO_{7-\delta}$, have been prepared. The X-ray data show that the tetragonal $n=2$ RP structure is retained across the series. Given the well-known difficulty of preparing $n=2$ RP phases that contain manganese and iron [10,13], it is not surprising that the compounds are both oxygen deficient and contain small impurities. While it is easy to form oxygen deficient $Sr_3Fe_2O_{7-\delta}$, our studies indicate that it is considerably more difficult to form a
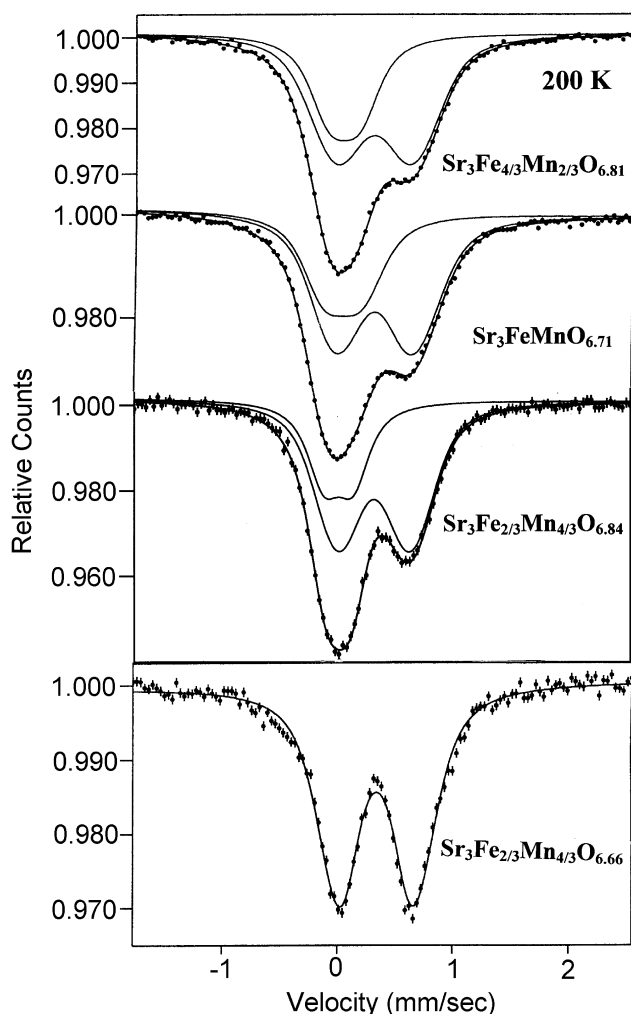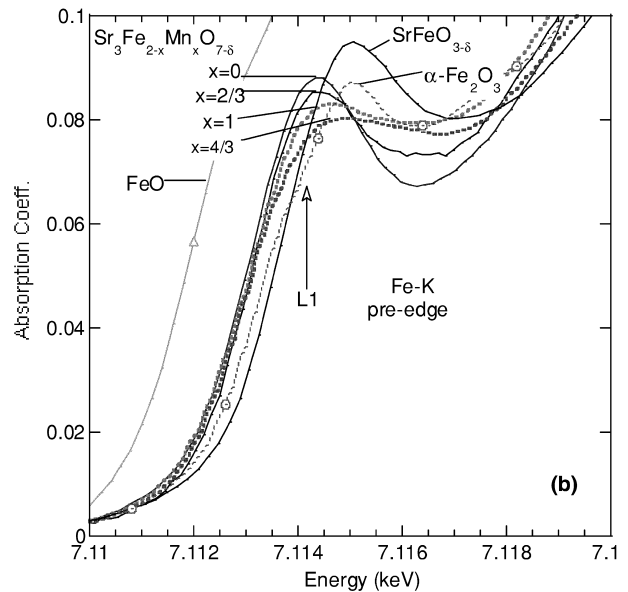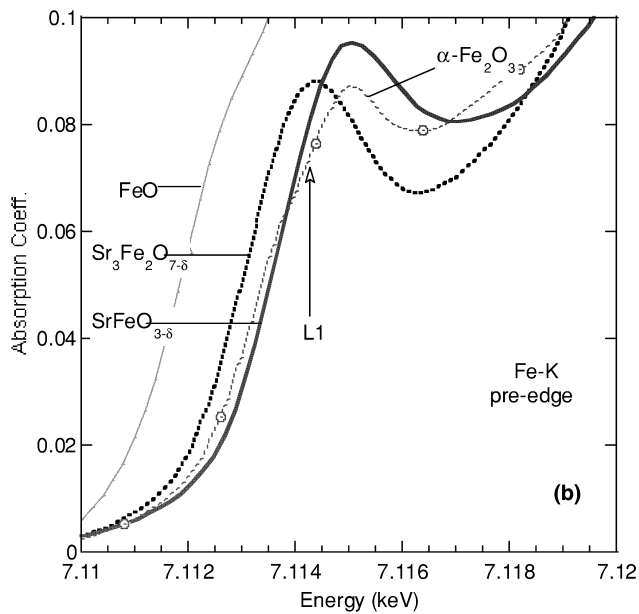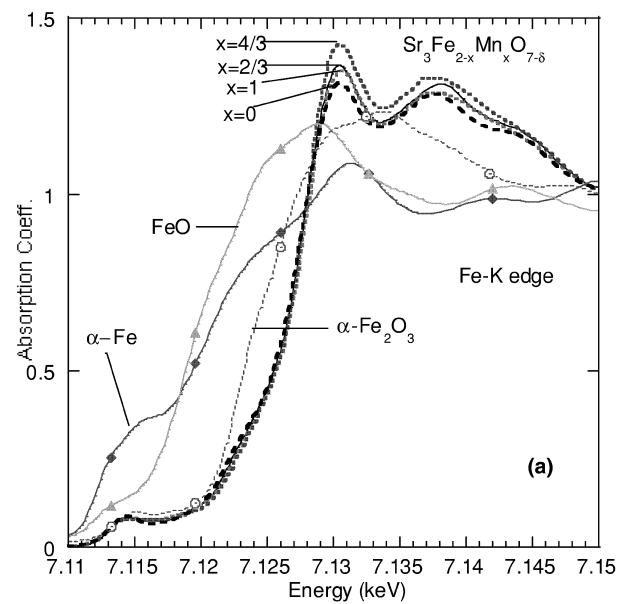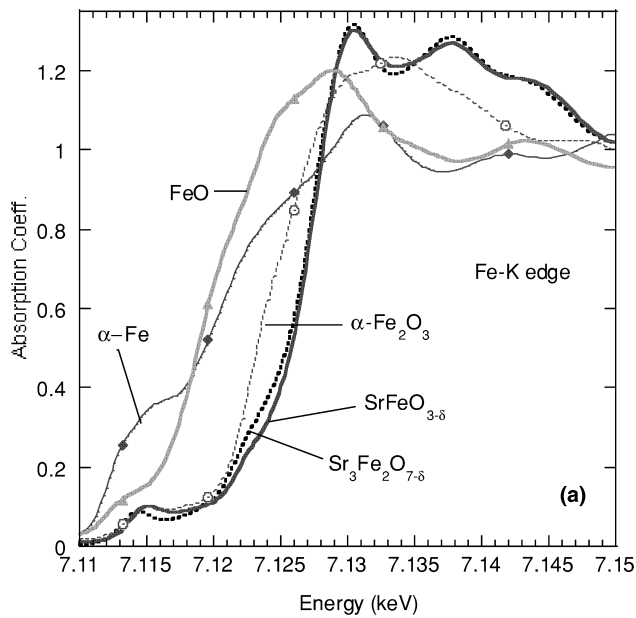
Fig. 7. (a) The Fe K-edges of $Sr_3Fe_2O_{7-\delta}$ and $SrFeO_{3-\delta}$; (b) the Fe K-pre-edges $Sr_3Fe_2O_{7-\delta}$ and $SrFeO_{3-\delta}$.

Fig. 8. (a) The Fe–K edges of $Sr_3Fe_{2-x}Mn_xO_{7-\delta}$ compounds along with those of the α-Fe, FeO and α-Fe_2O_3 standards. (b) The Fe–K pre-edges of $Sr_3Fe_{2-x}Mn_xO_{7-\delta}$ compounds along with those of the α-Fe, FeO and α-Fe_2O_3 and $SrFeO_{3-\delta}$ standards.

fully oxygenated RP iron compound. Due to the preparation techniques, all compounds contain O deficiencies, which introduce Fe^{3+} with concomitant effects on the physical properties. We anticipated that our samples would be oxygen deficient, and had planned to perform a soft oxidation reaction with a solution of $Br_2/NaOH$, but due to the moisture sensitivity of these compounds that was impossible. Annealing the samples in flowing oxygen in the TGA resulted in no weight gain.

For the $n=2$ RP phases, there is always the possibility of perovskite $n=\infty$ and $n=1$ intergrowths as well as stacking faults only visible under a high resolution electron

microscope (HREM) [18,19]. While our X-ray data does not show evidence of perovskite intergrowths, the small peaks from α-Sr_2MnO_4 and $Sr_4Mn_3O_{10}$ (see Fig. 2) indicate that the $n=2$ RP phases prepared here are iron rich. The EDAX data indicates that there is a homogeneous distribution of both iron and manganese throughout the sample. Attempts to sinter these compounds at higher temperature, $>1500°C$, resulted in slightly purer phases, but the samples were considerably more oxygen deficient. Iodometric titrations and Mössbauer data indicate that the iron is predominantly trivalent.
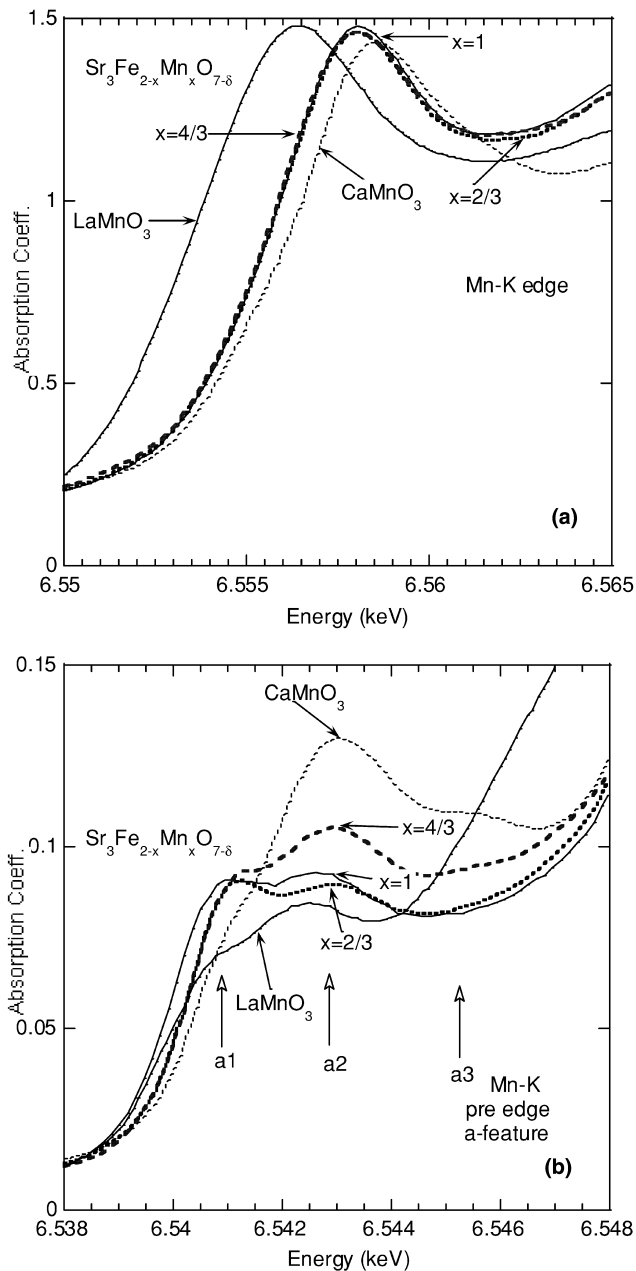
Fig. 9. (a) The Mn–K main edges of $Sr_3Fe_{2-x}Mn_xO_{7-\delta}$ ($x = 1/3$, 1/ and 4/3) compounds along with those of the $CaMnO_3$ and $LaMnO_3$ standards. (b) The Mn–K pre edges of $Sr_3Fe_{2-x}Mn_xO_{7-\delta}$ ($x = 1/3$, 1/ and 4/3) compounds along with those of the $CaMnO_3$ and $LaMnO_3$ standards.

Analysis of the magnetic data shows that the experimentally determined Curie constants are larger than the theoretically expected values. The larger than expected Curie constants have been observed in other studies [11,20], and have been attributed to FM clustering models at the high temperatures [11]. The experimentally determined θ values for the iron rich samples are positive, however, with increasing manganese content the θ values decrease, and it is negative for $x = 4/3$. This behavior suggests that there are FM interactions at high temperatures in the compounds

with relatively large iron concentrations, while AF interactions are dominant for those with high manganese content; the $x = 4/3$ sample orders AF around 50 K. It is difficult to interpret the complex magnetic structure of these compounds, due to the number of possible interactions between three magnetic ions. Depending on the oxygen defects and the ordering of the magnetic ions there could be AF Mn^{4+}–O–Mn^{4+}, Fe^{3+}–O–Fe^{3+}, Mn^{4+}–O–$Fe^{3+,4+,5+}$, and Fe^{3+}–O–Fe^{5+} super-exchange interactions; in addition direct metal-to-metal interactions, because of missing oxygen atoms, may also be important and could lead to AF or FM interactions depending on the local order around the metal ions. Because of the random distribution of transition metal ions, these compounds also exhibit spin-glass behavior. Although, there is long range magnetic order below 50 K for the $x = 4/3$ compound, a certain percentage of spins in this compound are disordered, hence the observed spin-glass like transition in Fig. 3. These complicated interactions could be best investigated with neutron diffraction techniques to understand where the oxygen defects are, as well as any magnetic ordering in the structure.

Mössbauer studies indicate that $SrFeO_{3-\delta}$ is primarily a Fe^{4+} compound, whereas $Sr_3Fe_2O_{7-\delta}$ at low temperatures [12] manifests a '$Fe^{3+/5+}$ charge disproportionation'. In fact the Mössbauer discussion emphasizes that the charge-site separation in this material is into temperature dependant $Fe^{[(4+)-\delta]}$ and $Fe^{[(4+)+\delta]}$ states as reinforced by the isomer shift versus valence correlations constructed in Fig. 10 from the data of Adler [11]. Indeed the continuous variation of the charge separation in the $Ca_{1-x}Sr_xFeO_3$ system further emphasizes the non-integral valence character of the states in such materials [21]. As already mentioned before, our analysis of the Mössbauer data shows similar results to those reported from the other studies [11,12,16]. The relative intensities of the sub-spectra in the Mössbauer data, assuming Fe^{3+}, Fe^{5+} and Mn^{4+}, are different than what we would expect from the oxygen content. This is believed to be associated with the incomplete disproportionation of the Fe^{4+} discussed by Adler [11]. The incomplete disproportionation is partially confirmed by the differences in the hyperfine fields and the isomer shifts between pure Fe^{3+} and Fe^{5+}, and those in our samples [11]. This low temperature disproportionation provides evidence into the nature of the complicated magnetic interactions that result when $2Fe^{4+}$ disproportionate into Fe^{3+} and Fe^{5+}.

The Fe–K main-edge XANES data in Fig. 7a show that, relative to $SrFeO_{3-\delta}$, the $Sr_3Fe_{2-x}Mn_xO_{7-\delta}$ spectrum does exhibit some additional weight on the low energy rising portion of the edge. The excess intensity on the low-energy side of the $Sr_3Fe_2O_{7-\delta}$ Fe–K edge spectrum (Fig. 7a) is suggestive of an enhanced lower valence component, however, one would have to say that the XAS results appear rather insensitive to the modest degree of charge separation in this material. In the Fe–K pre-edge feature in
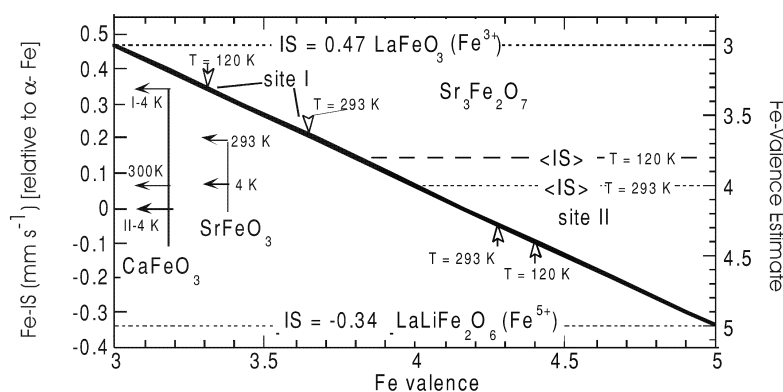
Fig. 10. Isomer shift versus Fe-valence results on $Sr_3Fe_2O_7$ from Adler [11]. Results from Takano et al. [16] on the homogeneous $SrFeO_3$ system and the 'disproportionated' $CaFeO_3$ system (300 K single site, and site I and II at 4 K). The nominal Fe-valence scale on the right is derived from the straight-line extrapolation (in the Figure) between the Fe^{3+} and Fe^{5+} standards as noted.

Fig. 7b, it is tempting to associate the shift in the L1-feature in the 327 compound, compared with that of the $SrFeO_{3-\delta}$, with the charge-separation occurring in the 327 compound. Specifically, the shift would be associated with the development of an L1-feature component at lower energy associated with Fe^{3+} admixture. Since such components are unresolved, the XANES pre-edge data can be viewed only as a suggestion.

The Fe-composition dependence of the Fe–K main edge in the $Sr_3Fe_{2-x}Mn_xO_{7-\delta}$ spectra (in Fig. 8a) does appear to indicate small variations in the main-edge peak position and the degree of broadening on the low-energy side of the steep edge rise. The changes with x in the Fe pre-edge are much stronger (see Fig. 8b) with the sharp-low-energy-peak (L1 in Fig. 8b) of the $x = 2/3$ spectrum being progressively rounded into a broadened shoulder with increasing x. This suggests transfer of spectral intensity from the L1 peak to higher energy. These spectral changes are quite dramatic, however the lack of current understanding of pre-edge behavior in Fe compounds underscores the need for theoretical work to comprehend such pre-edge features.

In detailed studies of the $La_{1-x}Ca_xMnO_3$ system ($0.2 < x < 1.0$) the Mn–K edge was shown to manifest a continuous chemical shift with increasing Mn valence [22]. $La_{1-x}Sr_xMnO_3$ ($0.2 < x < 0.5$) quantitatively manifests a very similar shift despite the changing shape of the peak in the Sr-substituted system. Taken at face value, the chemical shifts of the Mn–K spectral peaks in $Sr_3Fe_{2-x}Mn_xO_{7-\delta}$ ($x = 1/3$, 1/ and 4/3; Fig. 9a) suggest an average Mn valence in the 3.7–3.8 range. However the comparison to the $CaMnO_3$ standard reduces this observation to a proposal rather than an estimate.

Previous work has shown a direct correlation between the increase in the intensity of these pre-edge features and increase of the Mn-valence [22]. Again the spectral intensity of the $Sr_3Fe_{2-x}Mn_xO_{7-\delta}$ ($x = 1/3$, 1/ and 4/3) pre-edge features is intermediate between those of the Mn^{3+}–$LaMnO_3$ and the Mn^{4+}–$CaMnO_3$ standards. Again

this would support a Mn-valence that is less than Mn^{4+} in these Fe substituted materials. The pre-edge structure in these 327 materials is strikingly Fe concentration dependent (Fig. 9b). The Mn^{3+}–$LaMnO_3$ pre-edge exhibits an unresolved bimodal (a1/a2) structure with comparable intensities in the a1 and a2 sub-components (see Fig. 9b). In the Mn^{4+}–$CaMnO_3$ pre-edge the a1 feature is reduced to a shoulder, the a2 feature is very intense and a weak a3 feature has appeared (see Fig. 9b). The intensity of the a1-feature appears to grow, relative to the a2 feature, with increasing Fe substitution (x) in the $Sr_3Fe_{2-x}Mn_xO_{7-\delta}$ ($x = 1/3$, 1/ and 4/3) spectra. However, a simple valence change interpretation of this changing a1/a2 intensity ratio is not supported by the relatively x-independent, main-edge chemical shift.

Recent work suggested the association of the Mn–K pre-edge a1-feature with majority spin Mn-d-e_g states [23]. Thus, increase in the a1-feature intensity could be associated with increasing Mn-e_g localization upon Fe substitution. Since the Fe-e_g orbitals lie lower in energy, the Mn-e_g inter-site hopping would be expected to be reduced (localization increased) with increasing Fe substitution.

5. Conclusion

We were able to prepare metastable manganese substituted iron $n = 2$ RP phases $Sr_3Fe_{2-x}Mn_xO_{7-\delta}$ ($x = 1/3$, 1/ and 4/3). These compounds are not good candidates for CMR materials, because they do not undergo a paramagnetic-to-FM, or an insulator-to-metal transition. Due to the statistical distribution of a variety of magnetic ions in the lattice, Mn^{4+}, Fe^{3+}, Fe^{4+} and Fe^{5+}, super-exchange, rather than double-exchange interactions dominate. All of the compounds are highly insulating with spin-glass like behavior at low temperatures and antiferromagnetic ordering in $Sr_3Fe_{2/3}Mn_{4/3}O_{6.84}$ at around 50 K. Mössbauer data clearly show that the Fe^{4+} ions disproportionate into 'Fe^{3+}' and 'Fe^{5+}'. The XANES data are consistent with

the Mn valence close to, but possibly somewhat below $4+$ and a distribution of Fe oxidation states dependent on x.

References

[1] Kusters RM, Singleton J, Keen DA, McGreevy R, Hayes W. Physica B 1989;155:362.

[2] Rao CNR, Cheetham AK, Mahesh R. Chem Mater 1996;8:2421.

[3] Moritomo Y, Asamitsu A, Kuwahara H, Tokura Y. Nature 1996;380:141.

[4] Zener C. Phys Rev 1951;82:403.

[5] Ruddlesden SN, Popper P. Acta Cryst 1958;11:54.

[6] Gundakaram R, Arulraj A, Vanitha PV, Rao CNR, Gayathri N, Raychaudhuri AK, Cheetham AK. J Solid State Chem 1996;127:354.

[7] Huheey JH. In: Inorganic chemistry — principles of structure and reactivity, 2nd ed, New York: Harper and Row, 1978, pp. 71–4, ISBN 0-06-042986-0.

[8] Battle PD, Brandford WR, Mihut A, Rosseinsky MJ, Singleton J, Sloan J, Spring LE, Vente JF. Chem Mater 1999;11:674.

[9] Gallagher PK, MacChesney JB, Buchanan DNE. J Chem Phys 1966;45:2466.

[10] Dann SE, Weller MT, Currie DB. J Solid State Chem 1992;97:179.

[11] Adler P. J Solid State Chem 1997;130:129.

[12] Dann SE, Weller MT, Currie DB, Thomas MF, Al-Rawwas AD. J Mater Chem 1993;12:1231.

[13] Mitchell JF, Millburn JE, Medarde M, Short S, Jorgensen JD, Fernández-Díaz MT. J Solid State Chem 1998;141:599.

[14] Larson AC, von Dreele RB. GSAS–generalized crystal structure analysis system, Los Alamos National Laboratory, 1987, Report No. LA-UR-86-748.

[15] Licci F, Turilli G, Ferro P. J Magnet Magnet Mater 1996;164:L268.

[16] Takeda Y, Naka S, Takano M, Shinjo T, Takada T, Shimada M. Mater Res Bull 1978;13:61.

[17] Wang JT, Lin CL, Mihalisin T. J Appl Phys 1996;79:6608.

[18] Battle PD, Rosseinsky MJ. Curr. Opin. Solid State Mater. Science 1999;4:163.

[19] Sloan J, Battle PD, Green MA, Rosseinsky MJ, Vente JF. J Solid State Chem 1998;138:135.

[20] MacChessney JB, Sherwood RC, Potter JF. J Chem Phys 1963;43:1907.

[21] Takano M, Kawachi J, Nakanishi N, Takeda Y. J Solid State Chem 1981;39:75–84.

[22] Croft M, Sills D, Greenblatt M, Lee C, Cheong S-W, Ramanujachary KV, Tran D. Phys Rev B 1997;55:8726.

[23] Qian Q, Tyson TA, Kao C-C, Croft M, Cheong S-W, Greenblatt M. Phys Rev B, in press.